RSC Advances

RSC Publishing

PAPER

View Article Online
View Journal | View Issue

Cite this: *RSC Advances*, 2013, **3**, 17402

Plasma electrolysis allows the facile and efficient production of graphite oxide from recycled graphite†

Dang Van Thanh,[a] Hsiu-Cheng Chen,[a] Lain-Jong Li,[b] Chih-Wei Chu[c] and Kung-Hwa Wei*[a]

The production of graphite oxide from graphite usually requires strong oxidants, concentrated acids, and a reaction time of the order of 100 h. In this study, we adopted a highly efficient cathodic plasma (CP) process in which the vapor plasma envelope calorific effect provides instant oxidation and expansion of graphite for producing plasma-expanded graphite oxides (PEGOs) from recycled graphite electrodes (GEs) or high purity graphite (HG), within a reaction time of 10 min without the need for strong oxidants or concentrated acids. X-ray diffraction, X-ray photoelectron spectroscopy and Raman spectroscopy confirmed the dramatic structural change from GEs or HG to graphite oxides after the CP process. Furthermore, scanning electron microscopy and transmission electron microscopy revealed that the graphite oxide possessed a spheroidal morphology, with dimensions of 1–3 μm, as a result of melting and subsequent quenching during the plasma electrolysis process. We obtained a stable, homogeneous dispersion of PEGOs in *N*-methyl-2-pyrrolidone after sonication and filtering of the centrifuged PEGOs. We used these spheroidal graphite oxide particles as effective adsorbents for the removal of pollutants (*e.g.*, Methylene Blue) from aqueous solutions. These PEGOs also served as good precursors for the preparation of graphite nanoplatelets. CP processing appears to be an effective and environmentally friendly means for mass-producing graphite oxide.

Received 19th June 2013,
Accepted 22nd July 2013

DOI: 10.1039/c3ra43084g

www.rsc.org/advances

Introduction

Graphene, a single layer of carbon atoms bound together in a hexagonal lattice (*i.e.* a two-dimensional form of graphite),[1] has many potential applications in, for example, energy-storage materials,[2–5] polymer composites,[6–8] transparent conductive electrodes,[9–12] memory devices,[13–15] and sensors.[16–18] Several methods are available for preparing graphene: chemical vapor deposition (CVD),[19–21] epitaxial,[22,23] unzipping of carbon nanotubes,[24,25] electrochemical exfoliation,[26–29] liquid-phase exfoliation of graphite,[30,31] and chemical reduction of graphite oxide (GO).[32–34] Among these methods, the chemical reduction of GO is one of the most promising approaches for the large-scale production of graphene; it involves (i) oxidation of graphite to GO using the methods developed by Staudenmeier,[35] U. Hofmann,[36] or Hummers,[37] (ii) exfoliation of GO through ultrasonication or thermal treatment to yield graphene oxide; and (iii) chemical reduction of graphene oxide to a graphene or graphitic network of sp^2-hybridized carbon atoms. The mixtures of strong oxidants and concentrated acids used to prepare GO are, however, highly toxic and dangerously unstable, requiring additional safety precautions.[38,39] Moreover, the discharge of large quantities of acidic waste poses an environmental risk. Thus, new methods for the preparation of GO, without the need for toxic chemical agents or the harsh oxidation of graphite, would be of great interest from the perspectives of science, technology, and environmental protection. Hudson *et al.*[40] reported the preparation of GO from graphite using an electrochemical method with a reaction time on the order of several weeks; it would require further improvements if it were to become as effective as the chemical methods described above. Several other studies based on the electrochemical activation of glassy carbon (GC) or highly ordered pyrolytic graphite (HOPG) have also been reported for the successful formation of GO.[41,42] For each of these methods, however, graphite of relatively high purity (*e.g.* purified natural graphite, glassy carbon, or HOPG) is used as the starting material. To date, the preparation of GO using low-purity graphite such as graphite electrodes (GEs) that have been recycled from used batteries as the starting material has not yet been reported. Herein, we demonstrate a highly efficient, green, and facile approach—involving cathodic plasma (CP) processing and subsequent ultrasonication—for the synthesis of GO from GEs recycled from batteries.

[a]*Department of Material Science and Engineering, National Chiao Tung University, Hsinchu 300, Taiwan E-mail: khwei@mail.nctu.edu.tw*
[b]*Institute of Atomic and Molecular Sciences, Academia Sinica, Taipei, 11529, Taiwan*
[c]*Research Center for Applied Sciences, Academia Sinica, Taipei, 11529, Taiwan*

† Electronic supplementary information (ESI) available: A video of the cathodic plasma process is available in the supporting information. See DOI: 10.1039/c3ra43084g

A classic electrolysis reaction involves either an anode oxidation or a cathode reduction process in an electrolyte bath. In an electrolytic process, the onset of plasma can be triggered around the working electrode—so-called plasma electrolysis—when the applied voltage is larger than the threshold voltage, with a strong electric field generated near the working electrode (either the anode or cathode).[43–45] The plasma near the working electrode induces strong Joule heating in the vicinity of the submerged part of this electrode, resulting in the formation of a vapor plasma envelope (VPE) with a surrounding temperature exceeding 2000 °C.[44] Plasma electrolysis can, therefore, be used to enhance chemical or physical processes occurring on the electrodes. For example, plasma electrolytic oxidation in an electrolyte bath, where the working electrode is an anode having a surface area much smaller than that of the cathode, is widely used industrially for oxidizing metal surfaces to form metal oxide coatings.

In this present study, however, we applied a highly negative voltage (−60 V) from a DC power supply to a graphite working electrode, which we used as the cathode; when this graphite cathode approached, but barely reached, the surface of the electrolyte, plasma was generated instantly on the cathode (see the demonstration movies in the ESI†). If the graphite working cathode were submerged into the electrolyte at shallow depths (*e.g.*, 1 cm), no plasma was generated. We, therefore, term this plasma electrolysis process as a cathodic plasma (CP) process. Fig. 1 presents schematic representations of the equipment set-up that we used for the CP process in conjunction with an ultrasonication bath. Surprisingly, the surface of the graphite electrode tip that was covered by the generated plasma could be oxidized and exfoliated into the electrolyte in a controllable manner. One possible explanation for the mechanism in this CP process is that the enormous amount of heat generated from the VPE calorific effect supplied the thermal energy required for the local oxidation of the surface of the GE. Hence, this process could be used for oxidation of the GE or HG to produce graphite oxide without the need for a mixture of strong oxidants and concentrated acids; we term the material produced as plasma-expanded graphite oxide (PEGO). The entire experiment could be performed within 10 min at a temperature below 80 °C when using KOH and $(NH_4)_2SO_4$ in deionized (DI) water as the electrolytic solution. The detailed experimental conditions are described in the Experimental section.

With further ultrasonication of a solution of PEGO in NMP, we obtained exfoliated PEGO (EPEGO). In addition, during ultrasonication, a local hot spot of the VPE (spark) could induce instant exfoliation reactions, producing a small portion of graphene sheets or graphene-like materials. The major advantages of this CP approach for producing graphite oxide from graphite are a simple setup, low cost (GO can be derived from a plentiful resource: recycled GEs), rapid processing, and environmentally friendliness.

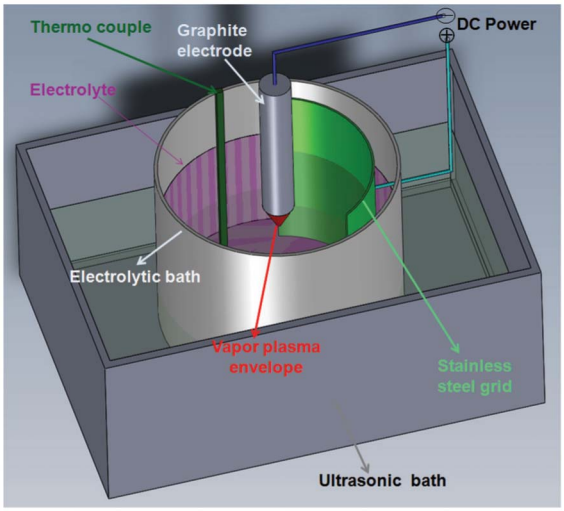

Fig. 1 Schematic representation of the equipment used for the CP process combined with ultrasonic vibration.

Experimental

Preparation of PEGO and PEHGO

The electrolytic solution, comprising KOH (10%, 180 mL) and $(NH_4)_2SO_4$ (5%, 20 mL) at a pH of approximately 14, was preheated to an initial temperature of 70 °C. A cylindrical graphite rod (GE) or high purity graphite (HG) was used as the cathode connected to a voltage supply unit (negative voltage output); the cathode diameter and length were 6 and 40 mm, respectively. A stainless-steel grid acted as the anode in the electrochemical system for the plasma expansion process (PEP). The top end of the cathode was placed about 1 mm above the surface of the electrolytic solution, while the anode was submerged in the electrolytic solution. The surface area of the cathode was much smaller than that of the anode as illustrated in Fig. 1a. Both electrodes were connected to a DC power supply (TES-6220) with an applied maximum fixed voltage of 60 V and a maximum current intensity of 3 A, resulting in a discharging plasma in the area adjacent to the GE and the electrolytic solution. As the exfoliation of GE progressed, the tip position of the GE was lowered to maintain a current of approximately 1.75 A. The temperature of the solution within the beaker was measured during the process using a conventional mercury thermometer; it was maintained at approximately 70–80 °C. To enhance exfoliation and the homogeneity of the reaction, the beaker containing the electrolytic bath was submerged partially in an ultrasonication bath maintained at 20 kHz under a power of 150 W. The length of time in which the samples experienced simultaneous treatment was 10 min. Fig. 1 provides schematic representations of the equipment set-up used in the CP process (also see the demonstration movies in the ESI†).

After CP treatment, the products were collected through vacuum filtration of the solution through PVDF membranes (average pore size: 0.2 μm) supported on a fritted glass holder. The resulting mixture was washed sequentially with DI water and 1% HCl and then repeatedly with DI water until the pH

reached 8. After drying at room temperature under vacuum for 24 h, the PEGO was obtained. The prepared samples were stored in a drying box at 50 °C until required for use. For comparing to the processing of recycled graphite electrode, we also applied the CP process to high purity graphite (HPG) for demonstrating the generality of the CP process, regardless of the starting graphite materials. The graphite oxides produced from the recycled graphite electrode (GE) and high purity graphite (HPG) are termed PEGO and PEHGO, respectively.

Preparation of EPEGO

The obtained PEGO (10 mg) was added to *N*-methyl-2-pyrrolidone (NMP, 100 mL) to create PEGO dispersion (0.1 mg mL^{-1}), which was subjected to exfoliation for 30 min using a tip ultrasonication apparatus (SONICS, 700 W, 75% amplitude). To remove unwanted large graphite particles produced during the exfoliation process, the resultant mixture was centrifuged for 5 min at 4000 rpm and then for 25 min at 1500 rpm. After centrifugation, the top 10 mL of the dispersion was decanted by pipette; herein, this sample is referred to as CGOD. The other resultant mixture was filtered through an AAO membrane (Anodisc; diameter: 47 mm, nominal pore size: 0.02 μm); the solids were then dipped in EtOH to remove residual NMP. The flakes that floated on the surface of the EtOH were collected on a Si substrate. After drying under vacuum at 50 °C for 24 h, a powdery product remained on the surface of the Si substrate; herein, it is named EPEGO.

Adsorption of MB on PEGO

The obtained PEGO powder (20 mg) was added to DI water (4 mL) to create a PEGO dispersion (5 mg mL^{-1}), which was added to MB solution (10 mg L^{-1}, 10 mL) and gently stirred before being left to equilibrate for 3 h. All experiments were performed at room temperature and a pH of approximately 7. After 3 h, a sample of the supernatant (2 mL) was removed by pipette to evaluate the residual MB concentration in the resultant solution. The amount of MB adsorbed was calculated using Beer's law, based on the absorption peak at 665 nm of the sample in a 1-cm quartz cell, as measured using a UV–Vis spectrophotometer.

Characterization

The structures of the GE, PEGO, PEHGO and EPEGO were examined using a D2 X-ray diffractometer equipped with a Cu-Kα tube and a Ni filter (λ = 0.1542 nm). Surface chemical compositions of PEGO and PEHGO were determined by XPS (Phi V6000). Raman spectra of these samples were recorded using a high-resolution confocal Raman microscope (HOROBA, Lab RAM HR) and a 632.8 nm HeNe laser source. UV–Vis spectra were recorded using a Hitachi U-4100 spectrophotometer. SAED patterns and HRTEM images were recorded using a JEOL 2100F apparatus operated at 200 kV; for HRTEM measurement, a few drops of the GE, HG, PEGO, HPEG and EPEGO solution were placed on a Cu grid presenting an ultrathin holey C film. SEM was performed using a JEOL JSM-6700F scanning electron microscope operated at 15 kV. Prior to SEM measurement, PEGO and HPEGO samples were coated with a thin (*ca.* 3 nm) layer of Pt. AFM images were obtained using a Digital Instruments Nanoscope III apparatus equipped with a NANOSENSORS Si tip, operated in the tapping mode with a resonance frequency of 130 kHz. AFM samples were prepared by drop-casting CGOD solutions onto the surfaces of Si/SiO_2 substrates and then drying in air.

Results and discussions

Fig. 2a presents X-ray diffraction (XRD) patterns of the GE, PEGO, and EPEGO samples. The diffraction curve of the GE displays a sharp, high-intensity peak near a value of 2θ of 26.6° that can be assigned to the characteristic peak (002) of graphite; this signal indicates a rather highly ordered crystal structure with a value of d_{002}, which is the spacing between two neighboring atomic planes in graphite, of 0.334 nm. In addition, weak peaks appear at values of 2θ of 21.5 and 23.5°, possibly resulting from some additives or impurities in the GE. After the GE had experienced the CP process, the characteristic (002) peak at a value of 2θ of 26.6° for PEGO almost disappeared completely, whereas the intensity of the diffraction peak at a value of 2θ of 9.8° (corresponding to a value of d_{001} of 0.896 nm), the characteristic (001) peak of GO, increased significantly, implying an increase in the interplanar distance: from 0.334 nm for GE to 0.896 nm for PEGO. This finding indicates that the original graphene layers in GE had lost their periodic arrangement in the z-direction after they had transformed into PEGO, an intercalated graphite compound,[46–48] through this CP process. For the EPEGO, the intensity of the characteristic (001) peak at a value of 2θ of 9.8° (d_{001} = 0.896 nm) decreased significantly, with a large peak appearing at a value of 2θ of approximately 26° (d_{002} = 0.341 nm). This d_{002} spacing for the EPEGO is close to the spacing of the characteristic (002) peak of GE (0.334 nm), indicating that the EPEGO contained exfoliated graphite sheets or graphite nanoplatelets. The presence of a peak for the EPEGO at a value of 2θ of 9.8° indicates, however, that a significant portion of PEGO had not been exfoliated.

Fig. 2b demonstrates the C 1s XPS spectrum of PEGO, where the peak at ~284.4 eV is attributed to the C=C (sp^2-hybridized carbon atoms) and the large and broad peak at ~286.4 eV is caused by C–O (hydroxyl and epoxy) groups along with two de-convoluted minor components at ~287.9 eV and at ~289.0 eV that resulted from C=O (carbonyl) and O–C=O (carboxylate carbon) groups, respectively, confirming the presence of graphite oxide and being consistent with the results of XRD.[33,49,50] Fig. 2c and 2d presented the XRD pattern and C 1s XPS spectrum of HPEGO, respectively. The peak at 2θ = 26.6° in the XRD curve of HPEGO sample confirms the presence of a substantial amount of the graphite phase, suggesting a lower conversion of high purity graphite (HG) into graphite oxide with the CP process than in the case of GE. In addition, the shoulder next to the C 1s XPS peak at 286 eV for the HPEGO samples can also be de-convoluted into four minor peaks at 284.6, 285.5, 286.1 and 286.9 eV that were attributed to C=C (sp^2-hybridized carbon atoms), C–C (sp^3-hybridized carbon atoms), C–O (hydroxyl group) and COOH (alcohol/ether groups), respectively, indicating graphite oxide-

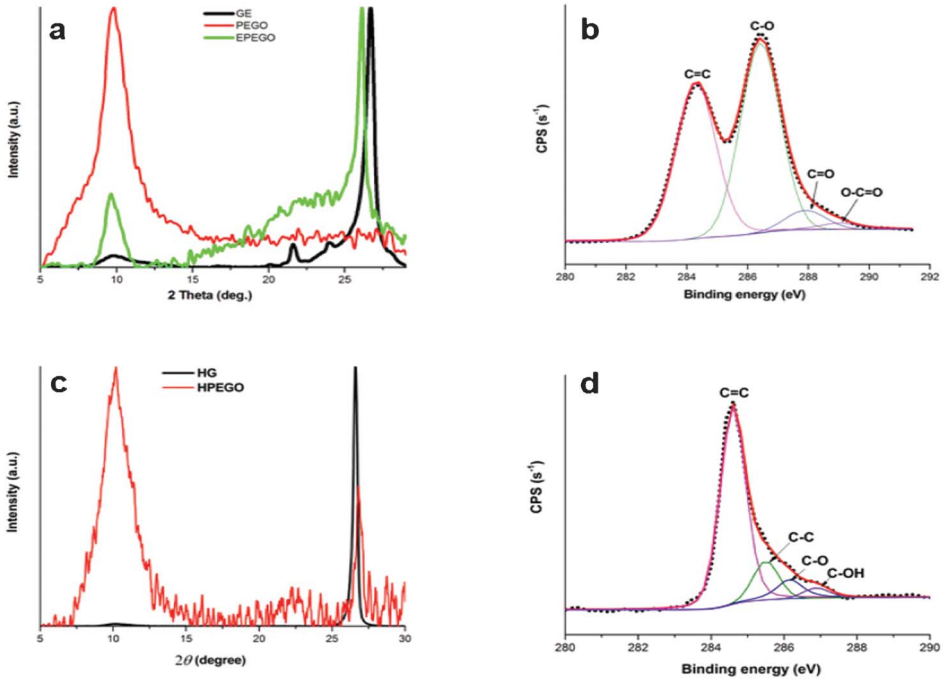

Fig. 2 (a) X-ray diffraction patterns of the GE, PEGO, and EPEGO samples, (b) X-ray photoelectron spectroscopy of C1s signal of PEGO, (c) XRD patterns of the HGO, HPEGO samples, and (d) X-ray photoelectron spectroscopy of C1s signal of HPEGO.

like structure.[33,38,50] Table 1 lists a quantitative comparison on the amounts of various oxygen containing groups in PEGO and HPEGO bases on the area under the XPS peaks. The atomic percentage of carbon in HPEGO (87%) is higher than that (43%) of PEGO, which translated to a carbon to the oxygen bonded carbon (C/O) ratio of 1.75 and 7.0, respectively, indicating that the CP process is more effective of generating GO from GE than from HG. This can be attributed to the more uniform packing of graphene layers in HG than in GE, as reflected in the much sharper (002) peak, at a value of 2θ of 26.6°, for the HG than that of the GE in the XRD curves.

Fig. 3 presents scanning electron microscopy (SEM) images of the GE, PEGO, and EPEGO samples, revealing their significantly different structures. Fig. 3a indicates that the GE in powder form consisted largely of multilayered graphite clusters. Fig. 3b reveals that the PEGO (see Fig. S2 in the ESI† for HPEGO), produced after the GE had been subjected to the CP process, featured crumpled structures and a heterogeneous surface, due to fast quenching; a high-magnification image of the PEGO (inset to Fig. 3b) indicates that it possessed spheroidal features having dimensions of 1–3 μm. The crumpled PEGO comprised many thin graphite oxide sheets, with the interactions among them being rather weak; thus, we expected it to undergo further exfoliation into thinner graphite oxide sheets. Fig. 3c reveals that the graphite oxide sheets, with lateral width from several hundreds of nanometers to 3 μm, could be produced after subjecting the PEGO to ultrasonication; the inset displays a magnified view of one such exfoliated sheet having a thickness (*ca.* 10–50 nm) close to the size of a nanoplatelet.[33] Image analysis calculations based on 20–50 EPEGO nanosheets revealed that the average sheet diameter was approximately 1.5 μm with a thickness of approximately 10–30 nm, based on cross-sectional imaging of the folded edges of EPEGO after tilting the sample from 0 to 25°. Notably, the EPEGO could be imaged clearly through SEM without the charging effects that occurred for PEGO.[33] Fig. 4 provides a schematic representation of our proposed mechanism for the formation of the PEGO. We considered that its shape was formed through the ''melting/quenching'' process displayed in Fig. 4a. During the CP process, the high-temperature plasma that existed in the regions close to the interfaces between the GE and the electrolyte supplied thermal energy for the oxidation of the GE. These regions of high-temperature plasma, however, were surrounded by the near room-temperature (70 °C) electrolyte; therefore, the temperature dropped rapidly across the interfaces, causing freezing of the oxidized features on the surface. The oxidized graphite clusters were then plucked from the surface of the GE and quenched in the electrolyte to form spherical and crumpled platelets that minimized the surface energy. Furthermore, the ultrasonic vibration enhanced the exfoliation of the outer shell of the oxidized GE. To verify this proposed mechanism, we

Table 1 The relative atomic percentage of various functional groups in PEGO and HPEGO estimated based on the area under the C 1s peaks

	C=C (%)	C–C (%)	C–O (%)	C–OH (%)	C=O (%)	O–C=O (%)
PEGO	43		50		5	2
HPEGO	74	13	9	4		

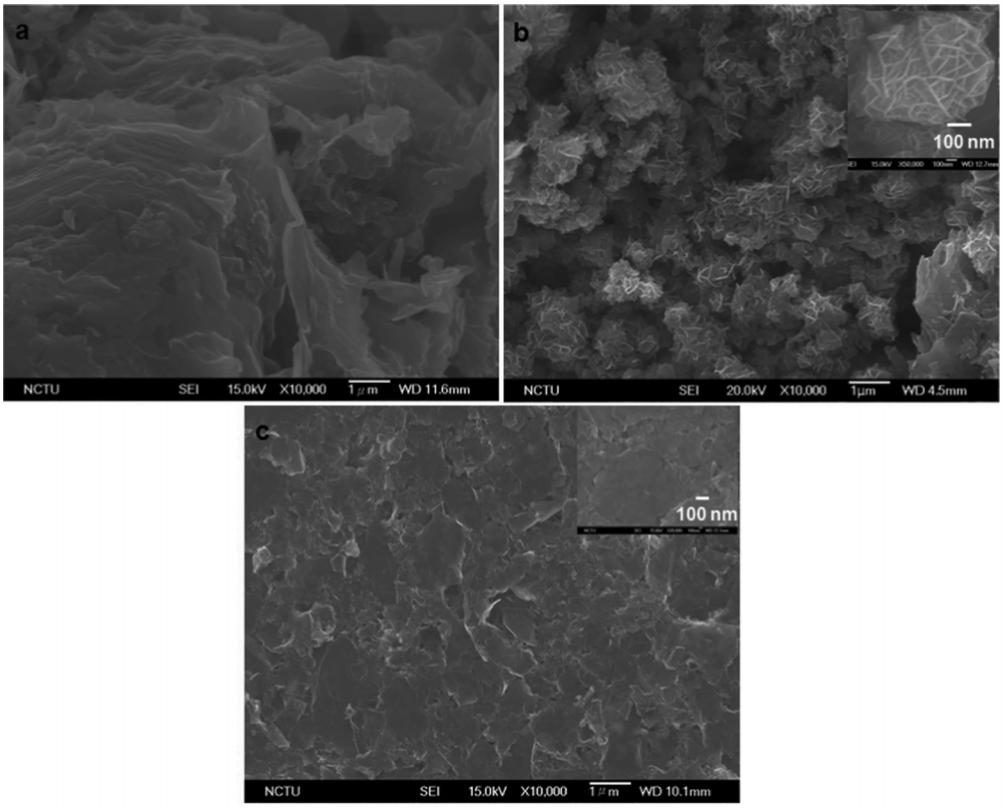

Fig. 3 SEM images of the (a) GE, (b) PEGO, and (c) EPEGO samples; insets: high-magnification images.

would need to accurately measure the temperature in the plasma region and perform a quantitative investigation of the prepared PEGO samples using various other characterization tools—experiments that are beyond the scope of this manuscript.

Fig. 4b displays a schematic representation of the detailed mechanism for the formation of graphite oxide from graphite when using this CP process. The plasma in the discharge channel can usually reach a very high temperature and pressure within a short period of time (*e.g.* $<10^{-6}$ s);[43] therefore, it is quite possible that when the surface of the GE cathode tip is surrounded by the VPE, which is generated in the interfacial areas between the electrolyte and the GE tip-surface, the GE tip-surface is rapidly heated to a high temperature (see the demonstration movies in the ESI†). As a result, the electrolyte in the vicinity of the GE tip-surface that was encompassed by the VPE in the plasma environment would be vaporized instantly, producing a number of active species, such as hydrogen or nitrogen radicals,[43,51,52] or oxygen-containing groups that could penetrate into the spaces between the graphene sheets in the VPE-encompassed GE tip. These radicals then attack the C–C bonds in the graphite to produce GO, resulting in their oxidation and expansion. This simultaneous oxidation and expansion in GE not only produces PEGO but also results in a 30-fold expansion in the spacing between two neighboring atomic planes in PEGO relative to that in the original GE.

Fig. 5 shows TEM images of GE, PEGO, HG, and HPEGO samples. Fig. 5a and 5b display micrometer-sized clusters with relatively thick, stacked aggregates of graphene layers for both GE and HG; Fig. 5c and 5d present images of a crumpled-like structure with inhomogeneous surfaces for PEGO and HPEGO after the GE and HG had experienced the CP process, being consistent with the SEM results.

Fig. 6a and 6b reveals the shapes, thicknesses, and lateral dimensions obtained from typical atomic force microscopy (AFM) images of the EPEGO; this EPEGO sample had a lateral dimension of approximately 250 nm and a thickness of approximately 4 nm, corresponding to approximately four layers of graphene, based on an interlayer spacing of 1 nm. Furthermore, the exfoliated EPEGO could be clearly identified in a high-resolution transmission electron microscopy (HRTEM) image, appearing translucent, with a selected area electron diffraction (SAED) pattern that reveals a typical hexagonally arranged lattice of carbon atoms. Two hexagonal patterns were overlapping each other, suggesting that the EPEGO samples comprised multi-layered graphene sheets, being consistent with Fig. 3c. The sizes and thicknesses of the nanoplatelets visualized in the HRTEM and AFM images were smaller than those in the SEM images, because the EPEGO samples had been diluted in NMP. These results suggest that PEGO can serve as a potential precursor for the preparation of graphite nanoplatelets. We suspect that optimizing the plasma power and ultrasonication conditions would allow us to

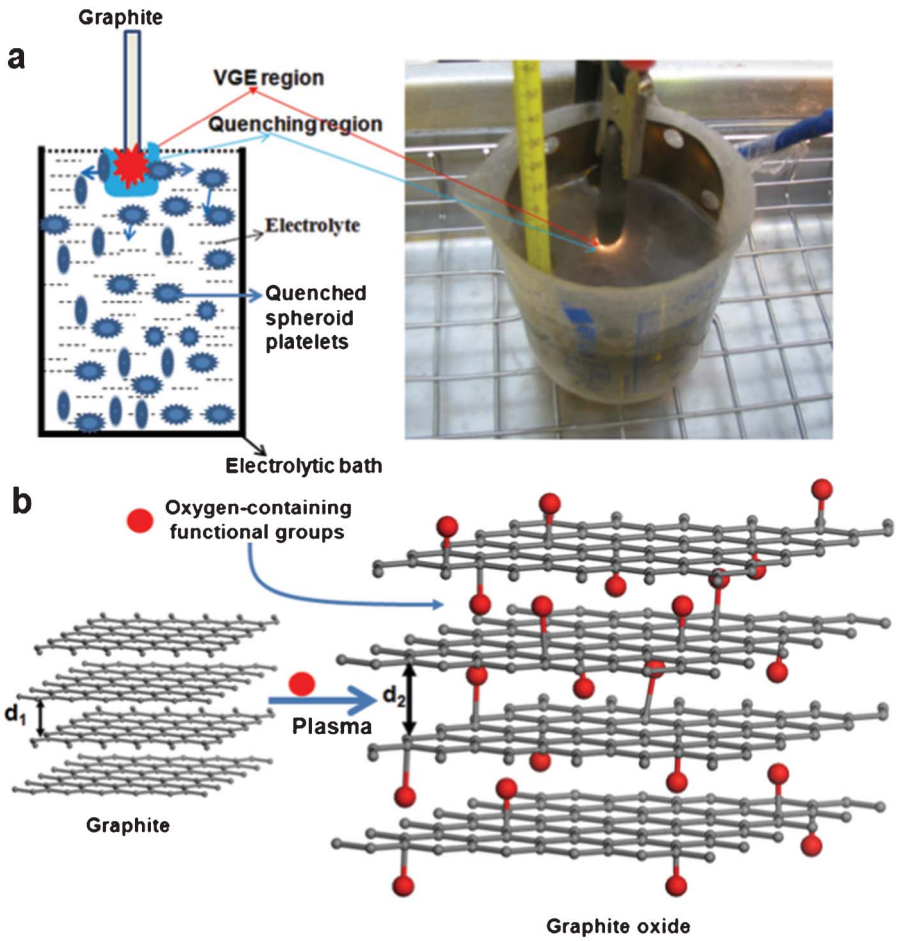

Fig. 4 (a) Mechanism of formation of PEGO and digital image of VPE. (b) Mechanism of plasma-mediated expansion of GE.

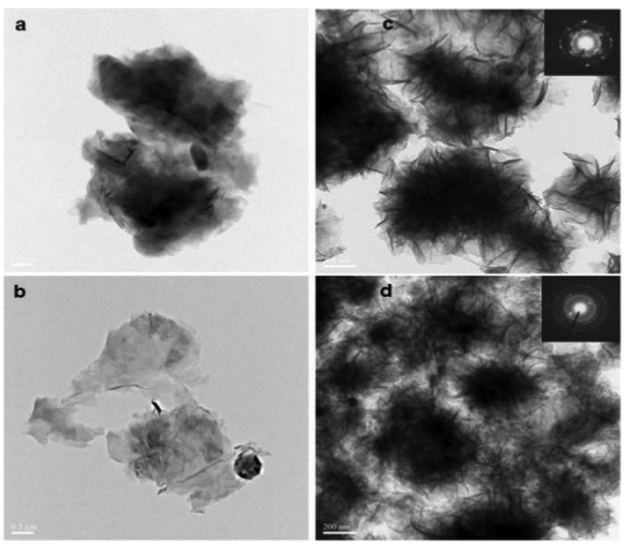

Fig. 5 TEM images of (a) GE, (b) HG, (c) PEGO, and (d) HPEGO; insets: corresponding SAED pattern.

control the lateral dimensions and thicknesses of these samples.

Fig. 7 displays Raman spectra of the GE, PEGO, and EPEGO samples, revealing their D (defect), G (graphite), and 2D (doubly generated G) bands at 1325, 1570, and 2658 cm^{-1}, respectively.[53,54] The D band of the GE has relatively high intensity, suggesting that the GE sample featured some defect structures, such as disordered carbon structures or impurities,[55] consistent with the XRD data. The peak positions of the D and G bands of the EPEGO sample are similar to those of the GE and PEGO samples, but the I_D/I_G intensity ratio for the EPEGO (0.53) was significantly lower than those (0.97) for both the GE and PEGO. Moreover, the intensity and sharpness of the G band of the EPEGO both increased significantly relative to those of the GE and PEGO samples, suggesting that disordered C structures, such as sp^3-hybridized C atoms, had been removed partially and that graphitic domains had been restored in the EPEGO sample during the ultrasonication process. In addition, the 2D band for EPEGO consisted of a single-Lorentzian 2D peak; its FWHM of approximately 70 cm^{-1} was, however, almost double that (*ca.* 35 cm^{-1}) of the 2D peak of graphene, consistent with the multilayer features of

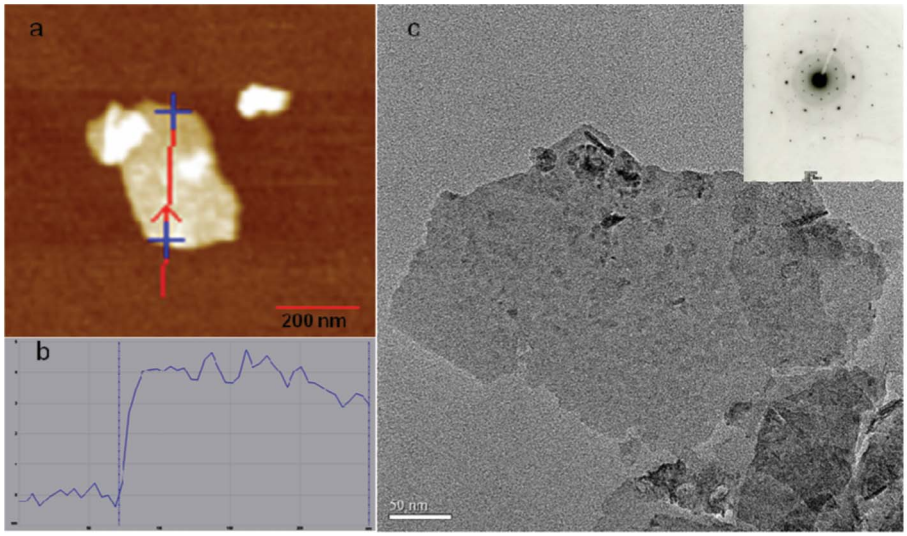

Fig. 6 (a) AFM image of a nanoplatelet of EPEGO deposited on a Si/SiO_2 substrate. (b) Line scan height profile of the sample in (a). (c) HRTEM image of an EPEGO nanoplatelet; inset: corresponding SAED pattern.

turbostratic graphene.[56] These results are consistent with the data from previous SEM and HRTEM studies.

The XRD, SEM, AFM, TEM and Raman data suggested that the PEGO served as a good precursor for the preparation of graphite nanoplatelets. Notably, when using VPE we could oxidize graphite without prior purification to remove additives or impurities, into GO within approximately 10 min, in contrast to the typically long treatment times (*ca.* 100 h) required when using concentrated acid and strong oxidizing agents. Taking into consideration the aspects of user-friendliness and recyclability, this VPE calorific process appears to be a very efficient means of synthesizing GO.

Fig. 8 displays photographs of dispersions of the PEGO in various solvents after performing the CP process. Fig. 8a reveals that some of the PEGO obtained from the CP process in the electrolyte solution precipitated to the bottom of the glass vial; Fig. 8b displays the PEGO sample obtained after filtering and re-dispersing in NMP without ultrasonication; Fig. 8c indicates that ultrasonication enabled the dispersion of PEGO in the NMP; and Fig. 8d reveals the clear PEGO/NMP solution obtained after centrifugation. Fig. 8c and 8d indicate that the PEGO solutions were rather homogeneous; they remained stable for long periods of time (12 weeks) with almost no precipitation.

To demonstrate the potential applications of PEGO materials, we applied the PEGO for the removal of Methylene Blue (MB) from aqueous solutions. Because the PEGO had a spheroidal structure, it could form 3D agglomerates with a large surface area,[57] making it a potentially useful absorbent. The inset to Fig. 9 reveals that an MB solution (10

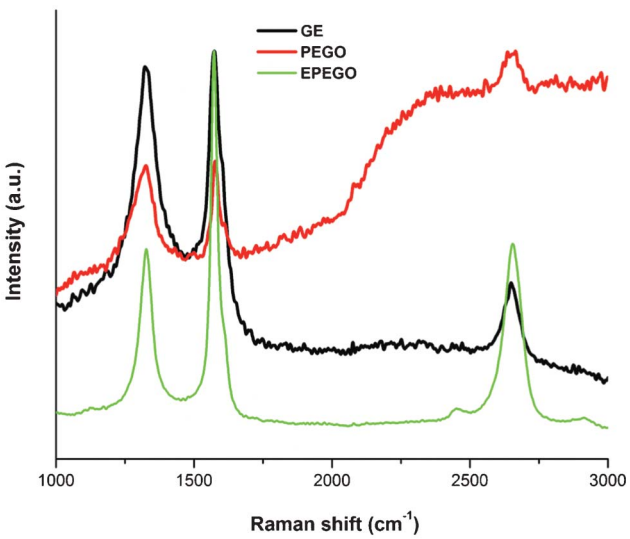

Fig. 7 Raman spectra of the GE, PEGO, and EPEGO samples.

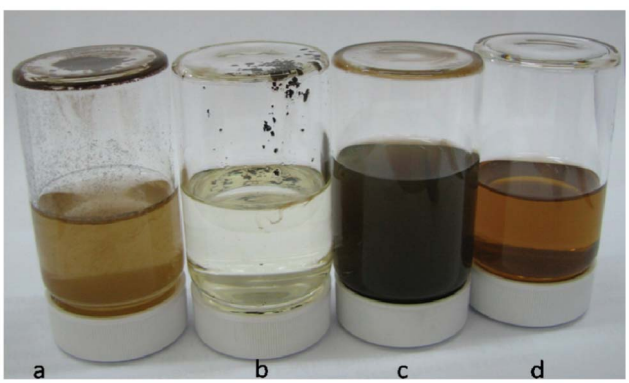

Fig. 8 Photograph of (a) the dispersion of PEGO in the electrolytic solution, (b) the sample obtained after filtering the sample in (a) through PVDF (pore size: 0.2 μm) and re-dispersion in NMP, (c) the sample obtained after ultrasonication of the sample in (b), and (d) the centrifuged dispersion of PEGO in NMP.

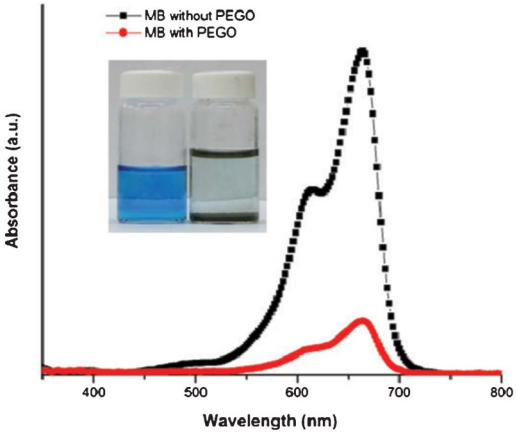

Fig. 9 UV–Vis spectra of MB solutions in the (red) presence and (black) absence of PEGO; inset: photograph of the (left) original MB solution and (right) MB-adsorbed PEGO solution.

mg L^{-1}, 10 mL), initially displaying a typical blue color, became a pale blue solution 3 h after addition of the PEGO solution (5 mg mL^{-1}, 4 mL), revealing that PEGO could remove MB efficiently with most of the MB-adsorbed PEGO having precipitated to the bottom of the glass container. After decanting the supernatant solution *via* pipette, we collected the aggregate and dried it at room temperature for 24 h. Notably, we applied the initial PEGO sample without any pretreatment. Fig. 9 displays UV–Vis spectra of the MB solution in the presence and absence of PEGO. We used the absorbance in each case to calculate the percentage adsorption of MB on the PEGO:

$$\text{Adsorption efficiency} = \left[\left[\frac{(A_i - A_f)}{A_i}\right] \times 100\right] (\%) \qquad (1)$$

where A_i and A_f are the initial and the final absorbances, respectively. The intensity of the characteristic peak at 665 nm for the MB solution that had been treated with the PEGO was dramatically lower than that of the pristine MB solution, indicating a significant drop in the concentration of MB in the solution; the removal efficiency, determined using eqn (1), was 97%. Therefore, our PEGO material appears to be a promising adsorbent for the removal of dyes or pigments, such as MB, from aqueous solutions.

Conclusions

Our characterization data reveal that swelled graphite oxide can be obtained from recycled graphite electrodes or even high purity graphite through a combination of cathodic plasma processing and ultrasonication at relatively low temperature, under atmospheric pressure, within a very short period of time, without the need for concentrated acids or strong oxidizing agents. The cathodic plasma process is a very efficient means of producing graphite oxide because it takes advantage of the vapor plasma envelope calorific effect that provides instant oxidation and expansion of graphite and appears to have great promise because it can be performed using various starting materials (*e.g.*, recycled graphites), at low cost, in a simple setup, and with high efficiency and environmental friendliness. The graphite oxide produced through this process can be used as an effective adsorbent for a removal of Methylene Blue from aqueous solutions and can serve as a suitable precursor for the preparation of graphite nanoplatelets.

Acknowledgements

This study was supported mainly by the National Science Council of Taiwan (NSC 101-3113-P-009-005). We thank Ms. Yu-Wei Chen for help with SEM imaging.

References

1 A. K. Geim and K. S. Novoselov, *Nat. Mater.*, 2007, **6**, 183.
2 J. Luo, H. D. Jang and J. Huang, *ACS Nano*, 2013, **7**, 1464.
3 M. Pumera, *Energy Environ. Sci.*, 2011, **4**, 668.
4 M. D. Stoller, S. Park, Y. Zhu, J. An and R. S. Ruoff, *Nano Lett.*, 2008, **8**, 3498.
5 G. Zhao, T. Wen, C. Chen and X. Wang, *RSC Adv.*, 2012, **2**, 9286.
6 S. C. Tjong, *Energy Environ. Sci.*, 2011, **4**, 605.
7 S. Bai and X. Shen, *RSC Adv.*, 2012, **2**, 64.
8 S. Stankovich, D. A. Dikin, G. H. B. Dommett, K. M. Kohlhaas, E. J. Zimney, E. A. Stach, R. D. Piner, S. T. Nguyen and R. S. Ruoff, *Nature*, 2006, **442**, 282.
9 S. Pang, Y. Hernandez, X. Feng and K. Müllen, *Adv. Mater.*, 2011, **23**, 2779.
10 C. L. Hsu, C. T. Lin, J. H. Huang, C. W. Chu, K. H. Wei and L. J. Li, *ACS Nano*, 2012, **6**, 5031.
11 X. Huang, Z. Zeng, Z. Fan, J. Liu and H. Zhang, *Adv. Mater.*, 2012, **24**, 5979.
12 T. K. Hong, D. W. Lee, H. J. Choi, H. S. Shin and B. S. Kim, *ACS Nano*, 2010, **4**, 3861.
13 Y. Ji, S. Lee, B. Cho, S. Song and T. Lee, *ACS Nano*, 2011, **5**, 5995.
14 J. Liu, Z. Yin, X. Cao, F. Zhao, L. Wang, W. Huang and H. Zhang, *Adv. Mater.*, 2013, **25**, 233.
15 A. J. Hong, E. B. Song, H. S. Yu, M. J. Allen, J. Kim, J. D. Fowler, J. K. Wassei, Y. Park, Y. Wang, J. Zou, R. B. Kaner, B. H. Weiller and K. L. Wang, *ACS Nano*, 2011, **5**, 7812.
16 J. Lin, D. Teweldebrhan, K. Ashraf, G. Liu, X. Jing, Z. Yan, R. Li, M. Ozkan, R. K. Lake, A. A. Balandin and C. S. Ozkan, *Small*, 2010, **6**, 1150.
17 T. Y. Chen, P. T. K. Loan, C. L. Hsu, Y. H. Lee, J. T. W. Wang, K. H. Wei, C. T. Lin and L. J. Li, *Biosens. Bioelectron.*, 2013, **41**, 103.
18 D. A. C. Brownson and C. E. Banks, *Analyst*, 2011, **136**, 2084.
19 A. Reina, X. Jia, J. Ho, D. Nezich, H. Son, V. Bulovic, M. S. Dresselhaus and J. Kong, *Nano Lett.*, 2008, **9**, 30.
20 D. Wei, B. Wu, Y. Guo, G. Yu and Y. Liu, *Acc. Chem. Res.*, 2012, **46**, 106.

21 C. Y. Su, A. Y. Lu, C. Y. Wu, Y. T. Li, K. K. Liu, W. Zhang, S. Y. Lin, Z. Y. Juang, Y. L. Zhong, F. R. Chen and L. J. Li, *Nano Lett.*, 2011, **11**, 3612.
22 A. Ouerghi, M. G. Silly, M. Marangolo, C. Mathieu, M. Eddrief, M. Picher, F. Sirotti, S. El Moussaoui and R. Belkhou, *ACS Nano*, 2012, **6**, 6075.
23 J. Robinson, X. Weng, K. Trumbull, R. Cavalero, M. Wetherington, E. Frantz, M. LaBella, Z. Hughes, M. Fanton and D. Snyder, *ACS Nano*, 2009, **4**, 153.
24 D. V. Kosynkin, A. L. Higginbotham, A. Sinitskii, J. R. Lomeda, A. Dimiev, B. K. Price and J. M. Tour, *Nature*, 2009, **458**, 872.
25 W. S. Kim, S. Y. Moon, N.-H. Park, H. Huh, K. B. Shim and H. Ham, *Chem. Mater.*, 2011, **23**, 940.
26 K. Parvez, R. Li, S. R. Puniredd, Y. Hernandez, F. Hinkel, S. Wang, X. Feng and K. Müllen, *ACS Nano*, 2013, **7**, 3598.
27 G. Wang, B. Wang, J. Park, Y. Wang, B. Sun and J. Yao, *Carbon*, 2009, **47**, 3242.
28 D. A. C. Brownson, D. K. Kampouris and C. E. Banks, *Chem. Soc. Rev.*, 2012, **41**, 6944.
29 C. Y. Su, A. Y. Lu, Y. Xu, F. R. Chen, A. N. Khlobystov and L. J. Li, *ACS Nano*, 2011, **5**, 2332.
30 Y. Hernandez, V. Nicolosi, M. Lotya, F. M. Blighe, Z. Sun, S. De, I. T. McGovern, B. Holland, M. Byrne, Y. K. Gun'Ko, J. J. Boland, P. Niraj, G. Duesberg, S. Krishnamurthy, R. Goodhue, J. Hutchison, V. Scardaci, A. C. Ferrari and J. N. Coleman, *Nat. Nanotechnol.*, 2008, **3**, 563.
31 E. K. Choi, I. Y. Jeon, S. Y. Bae, H. J. Lee, H. S. Shin, L. Dai and J. B. Baek, *Chem. Commun.*, 2010, **46**, 6320.
32 G. Wang, J. Yang, J. Park, X. Gou, B. Wang, H. Liu and J. Yao, *J. Phys. Chem. C*, 2008, **112**, 8192.
33 S. Stankovich, D. A. Dikin, R. D. Piner, K. A. Kohlhaas, A. Kleinhammes, Y. Jia, Y. Wu, S. T. Nguyen and R. S. Ruoff, *Carbon*, 2007, **45**, 1558.
34 H. Chen, M. B. Müller, K. J. Gilmore, G. G. Wallace and D. Li, *Adv. Mater.*, 2008, **20**, 3557.
35 L. Staudenmaier, *Ber. Dtsch. Chem. Ges.*, 1898, **31**, 1481.
36 U. Hofmann and E. König, *Z. Anorg. Allg. Chem.*, 1937, **234**, 311.
37 W. S. Hummers and R. E. Offeman, *J. Am. Chem. Soc.*, 1958, **80**, 1339.
38 H. L. Poh, F. Sanek, A. Ambrosi, G. Zhao, Z. Sofer and M. Pumera, *Nanoscale*, 2012, **4**, 3515.
39 D. C. Marcano, D. V. Kosynkin, J. M. Berlin, A. Sinitskii, Z. Sun, A. Slesarev, L. B. Alemany, W. Lu and J. M. Tour, *ACS Nano*, 2010, **4**, 4806.
40 M. J. Hudson, F. R. Hunter-Fujita, J. W. Peckett and P. M. Smith, *J. Mater. Chem.*, 1997, **7**, 301.
41 R. Bowling, R. T. Packard and R. L. McCreery, *Langmuir*, 1989, **5**, 683.
42 H. P. Dai and K. K. Shiu, *J. Electroanal. Chem.*, 1996, **419**, 7.
43 A. L. Yerokhin, X. Nie, A. Leyland, A. Matthews and S. J. Dowey, *Surf. Coat. Technol.*, 1999, **122**, 73.
44 P. Gupta, G. Tenhundfeld, E. O. Daigle and D. Ryabkov, *Surf. Coat. Technol.*, 2007, **201**, 8746.
45 T. Paulmier, J. M. Bell and P. M. Fredericks, *Thin Solid Films*, 2007, **515**, 2926.
46 H. Wang and Y. H. Hu, *Ind. Eng. Chem. Res.*, 2011, **50**, 6132.
47 Y. Zhao, G. S. Tang, Z. Z. Yu and J. S. Qi, *Carbon*, 2012, **50**, 3064.
48 A. Buchsteiner, A. Lerf and J. Pieper, *J. Phys. Chem. B*, 2006, **110**, 22328.
49 D. Cai and M. Song, *J. Mater. Chem.*, 2007, **17**, 3678.
50 H. K. Jeong, Y. P. Lee, R. J. W. E. Lahaye, M. H. Park, K. H. An, I. J. Kim, C. W. Yang, C. Y. Park, R. S. Ruoff and Y. H. Lee, *J. Am. Chem. Soc.*, 2008, **130**, 1362.
51 S. M. Thagard, K. Takashima and A. Mizuno, *Plasma Chem. Plasma Process.*, 2009, **29**, 455.
52 M. A. Mottaleb, J. S. Yang and H. J. Kim, *Appl. Spectrosc. Rev.*, 2002, **37**, 247.
53 F. Tuinstra and J. L. Koenig, *J. Chem. Phys.*, 1970, **53**, 1126.
54 A. C. Ferrari, J. C. Meyer, V. Scardaci, C. Casiraghi, M. Lazzeri, F. Mauri, S. Piscanec, D. Jiang, K. S. Novoselov, S. Roth and A. K. Geim, *Phys. Rev. Lett.*, 2006, **7**, 187401.
55 Y. Lu, Z. Zhu and Z. Liu, *Carbon*, 2005, **43**, 369.
56 D. R. Lenski and M. S. Fuhrer, *J. Appl. Phys.*, 2011, **110**, 013720.
57 J. Luo, H. D. Jang, T. Sun, L. Xiao, Z. He, A. P. Katsoulidis, M. G. Kanatzidis, J. M. Gibson and J. Huang, *ACS Nano*, 2011, **5**, 8943.

